Journal of Peptide Science

WILEY

Journal of PeptideScience

RESEARCH ARTICLE OPEN ACCESS

Cytosolic Delivery of Functional Ubiquitin

JoLynn B. Giancola[1] | Aniekan Okon[1] | Yanfeng Li[2] | Eric R. Strieter[2] | Ronald T. Raines[1]

[1]Department of Chemistry, Massachusetts Institute of Technology, Cambridge, Massachusetts, USA | [2]Department of Chemistry, University of Massachusetts Amherst, Amherst, Massachusetts, USA

Correspondence: Ronald T. Raines (rtraines@mit.edu)

Received: 12 February 2025 | **Revised:** 10 April 2025 | **Accepted:** 17 April 2025

Funding: This study was supported by the National Institutes of Health (F32 CA247259, R35 GM148220, R35 GM149532, and P30 CA014051).

Keywords: cytosol | delivery | endosomolytic peptide | proteostasis | traceless | ubiquitin

ABSTRACT

The proteostasis network involves complex protein signaling cascades. The tagging of proteins with ubiquitin is central to the degradation of cellular proteins, but understanding its exact role in processing proteins is complicated by the complexity and extent of its utilization within cells. Here, we describe the application of a traceless protein delivery strategy to effect the uptake of exogenous ubiquitin into the cytosol of human cells. We find that coadministration of the endosomolytic peptides L17E and, especially, L17ER$_4$ provides not only cytosolic access to ubiquitin but also its functional incorporation into endogenous proteins. By enabling the study of semisynthetic ubiquitin variants in the human cytosol, this strategy could advance the field of ubiquitin biology.

1 | Introduction

The proteasome is the key component of a tightly regulated network of ~2000 proteins that affect proteostasis [1, 2]. The dysregulation of proteostasis has been implicated in many diseases, heightening the importance of understanding the underlying biological chemistry [3]. Revelations could, for example, lead to novel therapies for aging and neurodegeneration [4, 5].

Ubiquitin is the key mediator of protein turnover in eukaryotic cells. Small (76 residues; 8.6 kDa) and neutral (p*I* 6.8), ubiquitin is used to tag proteins for degradation [6]. The linkage is an amide bond between the side-chain amino group of a lysine residue on the target protein and the main-chain carboxyl group of the C-terminal glycine residue of ubiquitin. Ubiquitin itself is rich in lysine residues, which can serve as sites for elaboration with additional ubiquitin monomers [7]. The connectivity of these linkages is important but complex [8]. After elaboration, ubiquitin-binding proteins recognize the linkage type and chain length of polyubiquitinated proteins, which directs appropriate processing by the proteasome [9]. Additional layers of cellular signaling are becoming apparent. The surface of ubiquitin can be elaborated with a variety of small-molecule signaling effectors, such as acetyl, amido, saccharide, or phosphoryl groups, to alter proteostasis [7, 10]. Changes in cell state are coordinated by the altered interactomes of modified ubiquitin proteins [7]. For example, mitophagy and the cellular response to DNA damage are regulated by the phosphorylation of ubiquitin at Thr12, Ser57, and Ser65 [11–14].

Because of its small size, ubiquitin is a candidate for chemical synthesis using solid-phase methods [15–17]. Total synthesis [18–20], the semisynthesis of ubiquitin with caged fluorophores [19, 21–23], and the preparation of ubiquitin-like proteins [24, 25] have been used to profile deubiquitinating enzyme activity and cellular processing in vitro and in live cells. The latter has been enabled by fusing ubiquitin to cell-penetrating peptides (CPPs) [26]. Protein chemistry has been used to install small-molecule sensors that enable the cellular tracking and proteome-wide profiling of interaction partners *in cellulo* [27–29]. Appreciation for the importance of the posttranslational modifications of ubiquitin on cells has

inspired the semisynthesis of ubiquitin variants with pendant arginine-rich CPPs and posttranslational modifications, as well as chemically defined ubiquitin dimers and tetramers [30–35]. These efforts have revealed the role of branching patterns on cellular processing [27] and the significance of phosphorylation on the proteostasis network [33].

Arginine-rich peptides are vulnerable to a high degree of endosomal entrapment and lysosomal degradation. In general, the uptake efficiency of CPPs is < 10%, which presents a high barrier to the cytosolic delivery of biomolecules [36, 37]. Moreover, the conjugation of a CPP to ubiquitin could impact its subcellular localization and, subsequently, its behavior. For these reasons, an efficient, traceless delivery method for the uptake of ubiquitin is desirable.

Endosomolytic peptides provide an alternative to CPPs. For example, the cotreatment of proteinaceous cargo with L17E, a rationally engineered endosomolytic peptide derived from Mlycotoxin [38, 39], enables efficient endosomal escape and cytosolic access [39–45]. Mechanistic studies reveal "carpet-like" membrane ruffling after macropinocytotic uptake [40]. Recently, we demonstrated that endosomolytic peptides can deliver highly anionic proteinaceous cargo to mammalian cells with high efficiency [46, 47]. We have also used this method to deliver peptide nucleic acids, which are neutral biomolecules of high therapeutic relevance [48]. Given our success with these challenging payloads, we sought to apply this delivery strategy to ubiquitin.

Here, we investigate the cytosolic uptake of ubiquitin upon coadministration with two endosomolytic peptides, L17E and $L17ER_4$ [44], and we explore its ability to function after entry (Scheme 1). We find that these two endosomolytic peptides affect the efficient cellular delivery of exogenously administered ubiquitin that can be processed by the cell.

2 | Materials and Methods

2.1 | Conditions

All procedures were performed at ambient temperature (~22°C) and pressure (1.0 atm) unless indicated otherwise.

2.2 | Materials

Commercially available reagents and solvents were reagent grade or better from Sigma–Aldrich (St. Louis, MO), unless specified otherwise, and were used directly without further purification. Amino acids were from Chem-Impex International (Wood Dale, IL). Rink Amide ProTide resin (LL) and Oxyma were from CEM Corporation (Matthews, NC). DIC and 4-methylpiperidine were from Oakwood Chemical (Tampa, FL). Water was obtained from a Milli-Q IQ 7000 purification system and had a resistivity of $18.2 \times 10^6\,\Omega\,\text{cm}$.

2.3 | Mass Spectrometry

The molecular mass of peptides was evaluated on a CHCA matrix with MALDI-TOF mass spectrometry with a microflex LRF instrument from Bruker (Billerica, MA). MALDI samples were desalted using DOWEX 50WX4-400 strong cation-exchange resin (CAS #11113-61-4) before spotting 1:1 v/v with the matrix. The molecular mass of proteins and protein conjugates was evaluated with a 6530C Accurate-Mass Q-TOF mass spectrometer equipped with a PLRP-S LC column (1000 Å, 5 μm, 2.1 × 50 mm) from Agilent Technologies. A gradient of 5%–95% v/v MeCN in water containing formic acid (0.1% v/v) over 7 min was used unless indicated otherwise. Before Q-TOF LC-MS analysis, samples were passed through a Corning Costar Spin-X centrifuge tube filter (0.22-μm cellulose acetate membrane) from R&D Systems (Minneapolis, MN).

2.4 | Peptide Synthesis

All amino acids used in solid-phase peptide synthesis (SPPS) were of L stereochemistry and were protected at their N terminus with fluorenylmethoxycarbonyl (Fmoc). Peptides were synthesized on Rink Amide ProTide Resin (LL) (0.1 mmol, 0.59 mmol/g, 1.0 equiv) with a Liberty Blue Automated Microwave Peptide Synthesizer from CEM Corporation (Matthews, NC) following the manufacturer's standard procedures. Solutions of Oxyma (1.0 M in DMF), DIC (0.5 M in DMF), 4-methylpiperidine (20% v/v in DMF), and Fmoc-protected amino acids (0.2 M in DMF) were used in coupling and deprotection steps.

Linear peptides with sequences listed in Table S1 were synthesized with single couplings of amino acid monomers as described previously [48]. When applicable, Fmoc-His(Boc)-OH was coupled for 10 min at 50°C under standard microwave conditions. After the synthesis, the resin was transferred to a 24-mL polypropylene Luer-lock syringe equipped with a filter frit.

After their syntheses, peptides were washed with DMF (5×) followed by DCM (15×) and were cleaved from the resin for 3 h using 2× the volume of DCM-swelled resin of cleavage cocktail, which contained TFA (82.5% v/v), H_2O (5% v/v), phenol (5% w/v), thioanisole (5% v/v), and 3,6-dioxa-1,8-octanedithiol (2.5% v/v). The

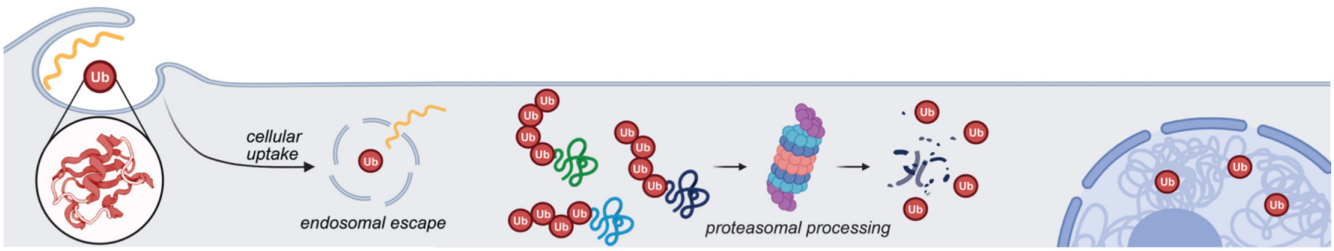

SCHEME 1 | Strategy overview: ubiquitin uptake and functional incorporation into live human cells.

resin was washed with an additional 4 mL of cleavage cocktail, and the pooled cleavage eluate was exposed to a stream of N_2(g) or Ar(g) to evaporate the cleavage cocktail. After concentration to a thick orange oil, the peptide was precipitated in 50 mL of ice-cold diethyl ether. The peptide was pelleted by centrifugation for 10 min at 1500 RPM at 4°C. The ether supernatant was decanted, and the crude peptide was stored at −70°C until purification.

2.5 | Peptide Purification

Peptides were purified by reversed-phase chromatography with a 1260 Infinity II Preparative LC System from Agilent Technologies (Santa Clara, CA) equipped with an XSelect Peptide CSH C18 OBD prep column (130 Å pore size, 5 μm particle size, 19 mm × 250 mm) from Waters (Milford, MA) or a VP 250/21 Nucleosil 100-5 C18 column from Macherey–Nagel (Düren, Germany). The crude peptide was reconstituted in a minimal amount of ACN, passed through a 0.22-μm PFTE filter, and separated using a gradient of 15%–40% v/v ACN in H_2O containing TFA (0.1% v/v) over 40 min. Purified fractions were pooled and lyophilized using a FreeZone benchtop instrument from Labconco (Kansas City, MO) to yield peptides as fluffy white TFA salts.

2.6 | Protein Chemistry

The A46C variant of human ubiquitin (UbA46C) was produced heterologously in *Escherichia coli*, as described previously [49]. UbA46C was characterized previously with Q-TOF LC-MS [47]. UbA46C was reconstituted at 395 μM in DPBS with Ca^{2+}/Mg^{2+}. TAMRA-PEG_2-maleimide from Broad Pharm (Product #24286) was reconstituted at 10 mM in DMSO. UbA46C was incubated with TAMRA-PEG_2-maleimide (1.1 equiv) in DPBS with Ca^{2+}/Mg^{2+} buffer system at pH 6.0 with shaking for 2 h. Reaction progress was monitored by Q-TOF LC-MS. When UbA46C was consumed, the excess dye was removed using Pierce Dye Removal Columns according to the manufacturer's recommendations. The UbA46C-TAMRA conjugate was exchanged into the reaction buffer of the subsequent step using either an Amicon Ultra 0.5-mL 10K MWCO Centrifugal Filter Unit or a 0.5-mL 7K MWCO Zeba Spin Desalting Column according to manufacturer's recommendations. UbA46C-TAMRA conjugate concentrations were assessed by the absorbance of the TAMRA dye.

2.7 | Biological Reagents, Supplies, and Instrumentation

Protein concentrations were determined with a DS-11 UV–vis spectrophotometer/fluorometer from DeNovix (Wilmington, DE). SDS-PAGE analyses were performed with Any kD Mini-PROTEAN TGX Precast Gels in a Mini-PROTEAN Tetra cell from Bio-Rad Laboratories (Hercules, CA). A Spectra Multicolor Broad Range Protein Ladder was from Thermo Fisher Scientific (Product #26634). Bio-Safe Coomassie G-250 Stain was from Bio-Rad Laboratories. A Titer Plate Shaker was from Labline Instruments (Melrose Park, IL). Gels were imaged with a ChemiDoc Gel Imager from Bio-Rad Laboratories. Pierce Dye Removal Columns were from Thermo Fisher Scientific (Product #22858). An Amicon Ultra 0.5-mL 10K MWCO Centrifugal Filter Unit was from MilliporeSigma (Burlington, MA) (Product #UFC501024). Zeba Spin Desalting Columns, 0.5-mL 7 KMWCO, were from Thermo Fisher Scientific (Product #89882).

HeLa cells were from ATCC (Product #CCL-2) and tested negative for mycoplasma. DMEM (high glucose and pyruvate) for HeLa cells was from Thermo Fisher Scientific (Product #11995065), as was FluoroBrite DMEM (Product #A1896701). Fetal bovine serum (FBS) was from Corning (Corning, NY) (Product #45001-108). Penicillin–streptomycin (10,000 U/mL) (Product #15140122) and trypsin–EDTA (0.25% w/v) with phenol (product #25200056) were from Thermo Fisher Scientific. DPBS with Ca^{2+}/Mg^{2+} (Product #14040141) and DPBS without Ca^{2+}/Mg^{2+} (Product #14190144) were from Gibco (Waltham, MA). SYTOX Blue dead-cell indicator was from Thermo Fisher Scientific (product #S34857). MG-132 proteasome inhibitor was from Sigma–Aldrich (Product #474790).

2.8 | Mammalian Cell Culture and Treatment Conditions

HeLa cells were grown in DMEM supplemented with FBS (10% v/v) and penicillin–streptomycin (1% v/v) in an incubator at 37°C and humidified with CO_2(g) (5% v/v). Cells were counted with a Countess II FL Automated Cell Counter (Product #AMQAF1000) and Countess Cell Counting Chamber Slides from Thermo Fisher Scientific (Product #C10283).

Identical cell seeding and treatment conditions were used across all cell studies. Cells were seeded to be 90% confluent at the time of the experiment. Specifically, cells were seeded at 36,000 cells/well if performing the experiment 24 h later, cells were seeded at 18,000 cells/well if performing the experiment 48 h later, and cells were seeded at 9000 cells/well if performing the experiment 72 h later. In each case, cells were seeded into an 18-well IbiTreat (#1.5 polymer coverslip, tissue culture treated, sterilized) plate (Product #81816) from Ibidi (Fitchburg, WI). Prior to treatment, cells were washed with DPBS without Ca^{2+}/Mg^{2+} (2 × 100 μL). The UbA46C-TAMRA conjugate was sterile-filtered with a Spin-X centrifuge tube filter. UbA46C-TAMRA constructs were used directly in cotreatment experiments. Constructs were prediluted to the appropriate treatment concentrations and subsequently dosed into each well according to the conditions listed in Table S2 in an incubator at 37°C humidified with CO_2(g) (5% v/v). The volume of the vehicle in each treatment condition did not exceed 20% of the medium volume, and the final volume of each well after the addition of an endosomolytic peptide and UbA46C-TAMRA was 40 μL. After incubation, cells were washed with DPBS without Ca^{2+}/Mg^{2+} (2 × 100 μL), and FluoroBrite DMEM (100 μL) was used for imaging. Cells were protected from light at room temperature until imaged.

2.9 | Epifluorescence Microscopy and Flow Cytometry

Cells were grown and treated according to the protocol in Section 2.8 and Table S2. A sequential epifluorescence

microscopy/flow cytometry workflow was adapted [46, 48] and deployed. Epifluorescence and differential interference contrast (DIC) live-cell images were acquired with an epifluorescence EVOS M7000 Imaging System (Product #AMF7000) from Thermo Fisher Scientific. The RFP light cube ($\lambda_{ex} = 531/40\,nm$, $\lambda_{em} = 593/40\,nm$) was used for excitation. Images were collected using standardized laser intensity values. Images were analyzed with the open-source Fiji distribution of ImageJ [50], adjusting for brightness and contrast, and processing was identically applied to all fluorescence images collected in a session.

After imaging, cells were washed with DPBS without Ca^{2+}/Mg^{2+} ($2 \times 100\,\mu L$) and lifted from the plate with $50\,\mu L$ of 0.25% v/v trypsin–EDTA. Trypsin was quenched by the addition of $50\,\mu L$ of complete medium. Cells were strained into flow tubes and pelleted by centrifugation for 5 min at 1000 RPM at 4°C. Cells were resuspended in 1 mL of ice-cold DPBS with Ca^{2+}/Mg^{2+} supplemented with BSA (0.1% w/v). Each sample was stained with SYTOX Blue dead-cell indicator ($1\,\mu L$ of a 1.0 mM stock) for ≥ 5 min on ice protected from light. Cells were kept on ice and protected from light until the time of analysis.

Flow cytometry measurements were made with a Life Technologies Attune NxT flow cytometer, which was equipped with 405-, 488-, 561-, and 640-nm lasers. The fluorescence intensity of at least 10,000 live events was measured by flow cytometry with an Attune NxT Flow Cytometer from Thermo Fisher Scientific. Control cells treated with SYTOX Blue ($1\,\mu L$ of a 1.0 mM stock) and cells treated with UbA46C-TAMRA (only) were analyzed first to set gates and laser intensities (Figure S4). For the SYTOX Blue signal, the 405-nm laser was used for excitation, and the 450/40 filter was used to detect fluorescence. For the TAMRA signal, the 561-nm laser was used for excitation, and the 585/16 filter was used to detect fluorescence. Events were collected using standardized laser intensity values. A template was established for laser intensity values, and all experiments were performed using these laser powers to enable comparison between data sets. Data were analyzed with the FlowJo software package from FlowJo (Ashland, OR) to obtain the MFI of live, single cells.

2.10 | Epifluorescence Microscopy Time-Course Imaging

Cells were grown and treated according to the protocol in Section 2.8 and Table S2. After a recovery period in an incubator at 37°C humidified with $CO_2(g)$ (5% v/v), cells were washed with DPBS without Ca^{2+}/Mg^{2+} ($2 \times 100\,\mu L$), and FluoroBrite DMEM ($100\,\mu L$) was used for imaging. Cells were protected from light at room temperature until imaged at 1, 6, and 24 h. After an imaging session, cells were washed with DPBS without Ca^{2+}/Mg^{2+} ($2 \times 100\,\mu L$), and full DMEM ($100\,\mu L$) was added to each well. Cells were returned to an incubator at 37°C humidified with $CO_2(g)$ (5% v/v). At the next time point, cells were prepared again in FluoroBrite DMEM ($100\,\mu L$).

2.11 | In-Gel Fluorescence Assay

HeLa cells were grown and treated according to the protocol in Section 2.8 and Table S2. After the recovery period, cells were treated with MG-132 ($10\,\mu M$). Cells were incubated overnight (≥ 16 h) prior to in-gel fluorescence analysis. Cells were then washed with DPBS without Ca^{2+}/Mg^{2+} ($2 \times 100\,\mu L$) and lifted from the plate with $50\,\mu L$ of 0.25% v/v trypsin–EDTA. Trypsin was quenched by the addition of $50\,\mu L$ of complete medium. Cells were transferred to 0.5-mL Eppendorf tubes and pelleted via centrifugation for 5 min at 1000 RPM at 4°C. Subsequently, cells were resuspended in $100\,\mu L$ of ice-cold DPBS with Ca^{2+}/Mg^{2+} as a wash and then pelleted again by centrifugation for 5 min at 1000 RPM at 4°C. Pellets were maintained on ice and protected from light.

Cells were lysed by using $20\,\mu L$ of RIPA lysis and extraction buffer from Thermo Fisher Scientific (Waltham, MA) (Product #89901), supplemented with Halt proteasome inhibitor cocktail (100×) from Thermo Fisher Scientific (Product #78438) and TCEP (100×) from Sigma–Aldrich (Product #646547). After the addition of the lysis buffer, cell samples were vortexed

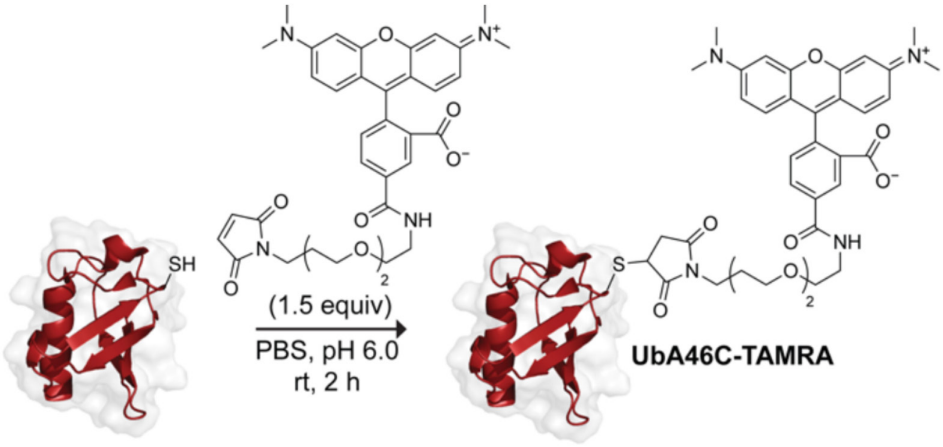

SCHEME 2 | Semisynthesis of a UbA46C-TAMRA conjugate.

briefly to resuspend the pellets, protected from light, and transferred to an orbital shaker maintained at 450 RPM at 4°C for 15 min to allow for cell lysis. After lysis, cells were subjected to centrifugation at 14,000*g* at 4°C to remove cellular debris. Supernatants (15 μL) were transferred to PCR strip tubes, and Fluorescent Compatible Sample Buffer (5 μL) from Thermo Fisher Scientific (Product #LC2570) was added to each sample. Samples were boiled for 5 min at 95°C and then loaded onto an Any-kD Mini-PROTEAN TGX gel from Bio-Rad (product #4569033). The SDS-PAGE gel was eluted at 195 V and 4°C for 30 min. Gels were imaged with a ChemiDoc imaging system from Bio-Rad using the AlexaFluor 546 Blot Channel and Auto Optimal Exposure.

3 | Results and Discussion

3.1 | Design and Semisynthesis of Fluorophore-Labeled Ubiquitin

To monitor the cellular delivery of ubiquitin, we sought a means to label ubiquitin with a fluorophore while preserving its ability to participate in endogenous signaling pathways. Because lysine is central to the branching of ubiquitin in cells, we avoided labeling with stochastic reagents that target amino groups. Fortunately, human ubiquitin does not contain any cysteine residues. Moreover, replacing Ala46 with a cysteine residue does not impact the processing of ubiquitin in the cell [49]. Accordingly, the cysteine in A46C ubiquitin (UbA46C) enables an orthogonal labeling strategy. As a fluorophore, we chose TAMRA because of its bright red fluorescence ($\lambda_{max} = 553$ nm; $\lambda_{em} = 575$ nm; $\Phi = 0.1$; $\varepsilon = 84{,}000\ M^{-1}\,cm^{-1}$) that is pH-agnostic, enabling a holistic appraisal of delivery efficacy. We produced UbA46C heterologously in *E. coli* as described previously (Figure S1) [49]. To install a single fluorogenic label on the protein, we reacted a TAMRA–maleimide fluorophore with the side-chain sulfyhydryl group of Cys46, yielding the UbA46C-TAMRA conjugate (Scheme 2 and Figure S2).

3.2 | Microscopy of Ubiquitin Internalization

We tested UbA46C-TAMRA (5 or 15 μM) along with a cotreatment of either L17E (40 μM) or L17ER$_4$ (20 μM) in HeLa cells. We first imaged these cells using epifluorescence microscopy to assess subcellular localization. Subsequently, we analyzed cells using flow cytometry to quantify uptake. We found that treatment conditions without serum afforded superior uptake (Figures S5 and S6). Microscopy revealed that UbA46C-TAMRA accessed the cytosol, as evidenced by diffuse fluorescent staining throughout the cytosol and nucleus of live HeLa cells (Figure 1A,B). We note the absence of punctate staining, which is indicative of endosomal entrapment. We observed an enhancement in cellular uptake and cytosolic access when cells were treated with higher concentrations of UbA46C-TAMRA, and we were gratified to observe that cellular uptake when cotreated with UbA46C-TAMRA was potentiated when treated with L17ER$_4$ (Figure 1A,B).

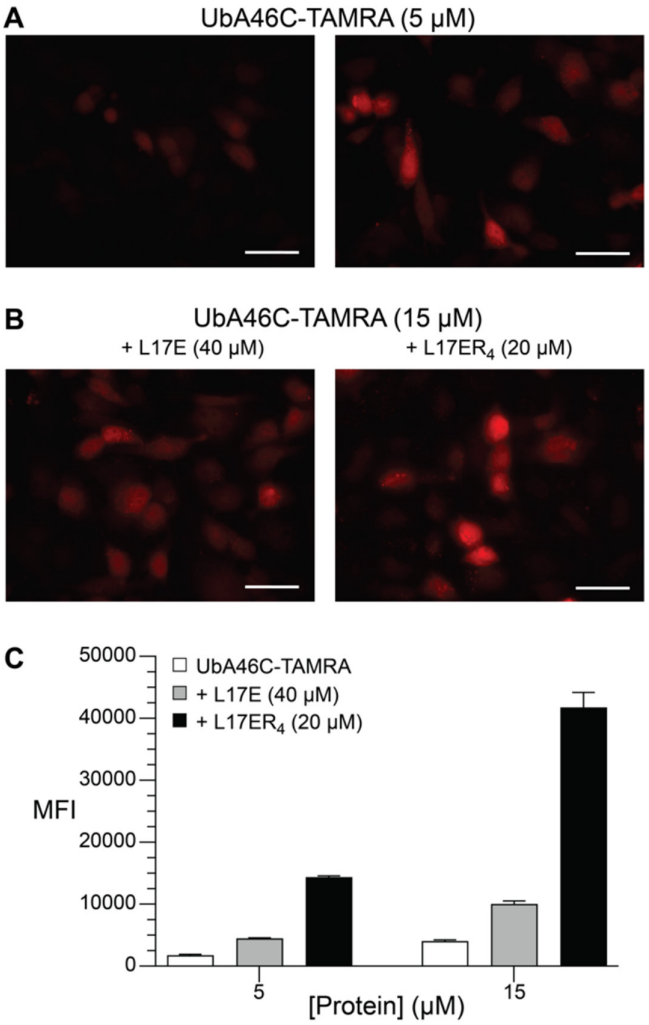

FIGURE 1 | Fluorescence microscopy and flow cytometry evaluation of UbA46C-TAMRA uptake in HeLa cells when cotreated with endosomolytic peptides L17E (40 μM) or L17ER$_4$ (20 μM) in serum-free DMEM. UbA46C-TAMRA uptake was evaluated by fluorescence microscopy at (A) 5 μM and (B) 15 μM after a 10-min serum-free cotreatment followed by a 1-h recovery in complete medium. Images are representative of uptake profiles of at least two independent experiments performed with two technical replicates. Scale bars, 50 μm. Additional images are shown in Figure S3. (C) MFI of UbA46C-TAMRA conjugates in HeLa cells was evaluated by flow cytometry. Values are the mean ± SE from at least two independent experiments, each performed with two technical replicates. Additional data are shown in Figures S5 and S6. Standardized laser intensities were used across all imaging and flow experiments.

3.3 | Cytometry of Ubiquitin Internalization

Flow cytometry enabled quantification of UbA46C-TAMRA uptake (Figure 1C). We observed that cells treated with UbA46C-TAMRA (5 μM) and cotreated with L17ER$_4$ (20 μM) had an approximately threefold increase in uptake compared to cells cotreated with L17E (40 μM). At a higher concentration of UbA46C-TAMRA (15 μM), L17ER$_4$ was approximately fourfold more effective than L17E. We consistently observed that when cells were cotreated with L17E, only ~35% of cells

had taken up UbA46C-TAMRA (Figure S6). In contrast, ~85% of cells cotreated with L17ER$_4$ demonstrated a change in fluorescence, and the magnitude of the shift in population was intensified with higher concentrations of UbA46C-TAMRA (Figure S6). Taken together, these results assert L17ER$_4$ as the superior endosomolytic peptide in affording cytosolic access to UbA46C-TAMRA.

3.4 | Time Course of Ubiquitin Internalization

With conditions in hand to enable robust cellular entry of UbA46C-TAMRA, we performed a time-course imaging experiment using UbA46C-TAMRA (15 μM) cotreated with L17ER$_4$ (20 μM) to observe changes in subcellular localization of our fluorogenic ubiquitin protein. We observed changes in subcellular localization that suggested the utilization of the conjugate by the cell (Figure 2). We evaluated cellular localization after 1, 6, and 24 h. After 1 h, we observed cytosolic and nuclear staining, consistent with successful cellular entry. After 6 h, fluorescence persisted in the nucleus and cytosol, suggesting that the exogenously administered material was utilized by the cell for nuclear proteolysis or, possibly, transcriptional programming [51]. Previous reports have likewise revealed nuclear sequestration after cytosolic delivery [27, 52]. At longer time points, we observed the appearance of fluorescent puncta, which could be consistent with either the utilization of the exogenous ubiquitin by the proteasome or by the degradation of the surplus of this protein. Broadly, we noted that the cell appeared to process the ubiquitin conjugate in accord with established ubiquitin biology.

3.5 | Cellular Processing of Internalized Ubiquitin

Next, we sought to assess the cellular processing of the exogenously administered ubiquitin conjugate. To do so, we used a gel-based assay to assess proteome-wide ubiquitin utilization. A measure of success was the fluorescent labeling of high molecular weight proteins, which corresponds to protein tagging with our probe.

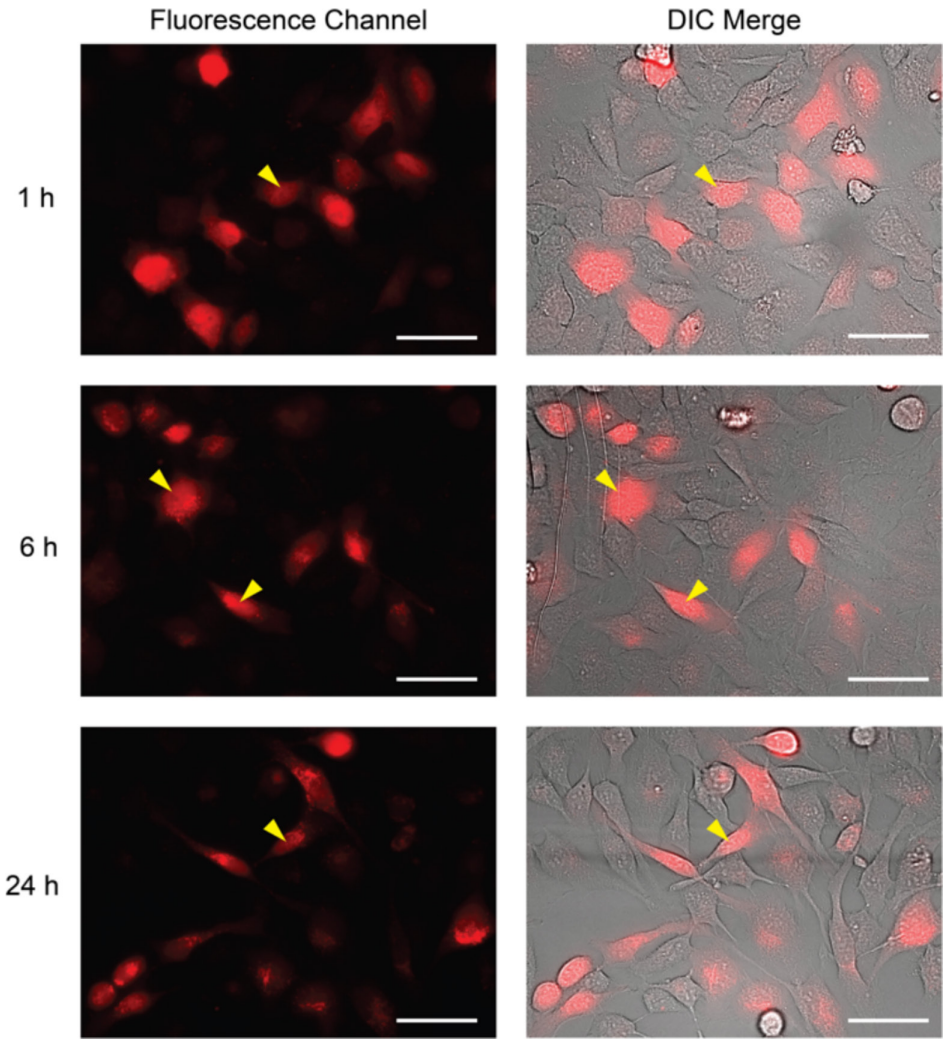

FIGURE 2 | Time-course fluorescent and transmitted light imaging of live HeLa cells cotreated with UbA46C-TAMRA (15 μM) and L17ER$_4$ (20 μM) in serum-free DMEM, normalized to cells treated with UbA46C-TAMRA only. All images were acquired with identical laser settings. Images are representative of at least two independent experiments with two technical replicates. Scale bars, 50 μm. Additional images are shown in Figure S7. Yellow arrows indicate the location of nuclei in select cells.

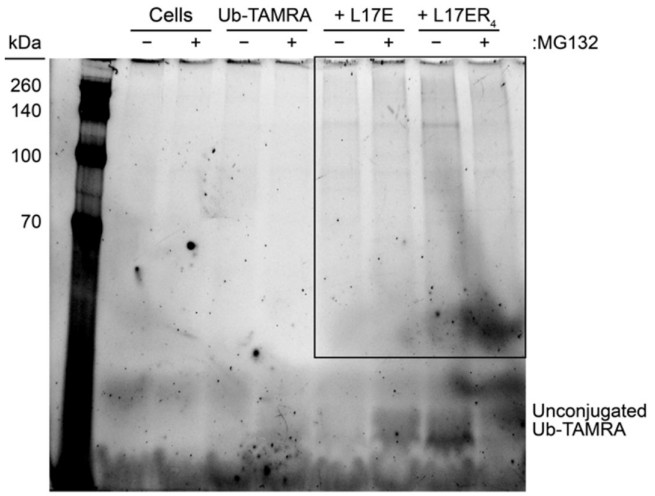

FIGURE 3 | Fluorescence of an SDS–PAGE gel of HeLa cell lysates after a 10-min treatment in serum-free medium with UbA46C-TAMRA (15 μM) alone or UbA46C-TAMRA (15 μM) and either L17E (40 μM) or $L17ER_4$ (20 μM) and an overnight recovery period in complete medium in the absence or presence (−/+) of MG132 (10 μM). The area in the box is indicative of ubiquitin conjugates. Additional data are shown in Figure S8.

Using the same treatment conditions that were identified previously, cells were cotreated with UbA46C-TAMRA (15 μM) and either L17E (40 μM) or $L17ER_4$ (20 μM) for 10 min in serum-free medium in an incubator at 37°C humidified with CO_2(g) (5% v/v). Cells were then washed and permitted to recover for 1.5 h prior to the addition of MG132 (10 μM), which is a peptidic proteasome inhibitor [53]. The treated cells were incubated overnight to allow for the enrichment of labeled proteins within the cells, lysed, and evaluated for ubiquitin incorporation using fluorescent imaging after separation on an SDS-PAGE gel.

Gratifyingly, we observed the appearance of fluorescent signals in slowly migrating proteins, indicating that exogenously delivered UbA46C-TAMRA was utilized by the proteasome (Figure 3). Both endosomolytic peptides afforded evidence of incorporation, but we observed a stronger fluorescence signal with $L17ER_4$ than L17E. These results are in accord with our microscopy and flow cytometry data, which likewise indicate that $L17ER_4$ provides greater cytosolic access. MG132 [53] did not appear to potentiate ubiquitin incorporation, perhaps due to synergistic cytotoxicity upon treatment along with endosomolytic peptides. Due to increased cytotoxicity under these treatment conditions, the number of lysed cells analyzed on the gel was lower. Thus, the magnitude of fluorescence could not exceed that of cells treated with the endosomolytic peptide alone. Nevertheless, UbA46C-TAMRA enrichment above background is observed in these samples.

4 | Conclusions

Ubiquitin is a linchpin for proteostasis within eukaryotic cells. We report a facile means for the traceless delivery of exogenous ubiquitin to the cytosol of human cells. The method deploys cotreatment with an endosomolytic peptide. The delivered ubiquitin is competent for conjugation to cellular proteins, a tag that entices degradation by the proteasome. This strategy is poised to illuminate underexplored aspects of ubiquitin biology, including the role of ubiquitin posttranslational modifications.

Acknowledgments

The authors thank the High Throughput Facilities Core of the Koch Institute for Integrative Cancer Research at MIT for providing the HeLa cell line and performing mycoplasma testing. We are grateful to Prof. Laura L. Kiessling (MIT) for helpful discussions and for the use of her ChemiDoc Gel Imager. Some graphics were created with BioRender. Open Access funding enabled and organized by MIT Hybrid 2025.

Conflicts of Interest

The authors declare no conflicts of interest.

Data Availability Statement

The data that support the findings of this study are available in the Supporting Information.

References

1. G. A. Collins and A. L. Goldberg, "The Logic of the 26S Proteasome," *Cell* 169 (2017): 792–806.

2. M. S. Hipp, P. Kasturi, and F. U. Hartl, "The Proteostasis Network and Its Decline in Ageing," *Nature Reviews. Molecular Cell Biology* 20 (2019): 421–435.

3. R. B. Damgaard, "The Ubiquitin System: From Cell Signalling to Disease Biology and New Therapeutic Opportunities," *Cell Death and Differentiation* 28 (2021): 423–426.

4. R. C. Taylor and A. Dillin, "Aging as an Event of Proteostasis Collapse," *Cold Spring Harbor Perspectives in Biology* 3 (2011): a004440.

5. J. Labbadia and R. I. Morimoto, "The Biology of Proteostasis in Aging and Disease," *Annual Review of Biochemistry* 84 (2015): 435–464.

6. C. M. Pickart, "Mechanisms Underlying Ubiquitination," *Annual Review of Biochemistry* 70 (2001): 503–533.

7. I. Dikic and B. A. Schulman, "An Expanded Lexicon for the Ubiquitin Code," *Nature Reviews. Molecular Cell Biology* 24 (2022): 273–287.

8. K. A. Andersen, L. J. Martin, J. M. Prince, and R. T. Raines, "Intrinsic Site-Selectivity of Ubiquitin Dimer Formation," *Protein Science* 24 (2015): 182–189.

9. R. Agrata and D. Komander, "Ubiquitin—A structural Perspective," *Molecular Cell* 85 (2025): 323–346.

10. L. T. Henneberg and B. A. Schulman, "Decoding the Messaging of the Ubiquitin System Using Chemical and Protein Probes," *Cell Chemical Biology* 28 (2021): 889–902.

11. F. Koyano, K. Okatsu, H. Kosako, et al., "Ubiquitin Is Phosphorylated by PINK1 to Activate Parkin," *Nature* 510 (2014): 162–166.

12. K. Okatsu, Y. Sato, K. Yamano, et al., "Structural Insights Into Ubiquitin Phosphorylation by PINK1," *Scientific Reports* 8 (2018): 10382.

13. K. N. Swatek, J. L. Usher, A. F. Kueck, et al., "Insights Into UBIQUITIN Chain Architecture Using Ub-Clipping," *Nature* 572 (2019): 533–537.

14. N. L. Hepowit, C. C. Kolbe, S. R. Zelle, E. Latz, and J. A. Macgurn, "Regulation of Ubiquitin and Ubiquitin-Like Modifiers by Phosphorylation," *FEBS Journal* 289 (2022): 4797–4810.

15. D. S. Hameed, A. Sapmaz, and H. Ovaa, "How Chemical Synthesis of Ubiquitin Conjugates Helps to Understand Ubiquitin Signal Transduction," *Bioconjugate Chemistry* 28 (2017): 805–815.

16. S. M. Mali, S. K. Singh, E. Eid, and A. Brik, "Ubiquitin Signaling: Chemistry Comes to the Rescue," *Journal of the American Chemical Society* 139 (2017): 4971–4986.

17. M. Pan, Q. Zheng, S. Ding, et al., "Chemical Protein Synthesis Enabled Mechanistic Studies on the Molecular Recognition of K27-Linked Ubiquitin Chains," *Angewandte Chemie, International Edition* 58 (2019): 2627–2631.

18. J. Liang, G. Fang, X. Huang, et al., "Chemical Synthesis of Ub-AMC via Ligation of Peptide Hydrazides," *Science China. Chemistry* 56 (2013): 1301–1306.

19. L. Xu, Y. Xu, Q. Qu, et al., "Efficient Chemical Synthesis for the Analogue of Ubiquitin-Based Probe Ub–AMC With Native Bioactivity," *RSC Advances* 6 (2016): 47926–47930.

20. P. Ghosh, "Boronic Acid-Linked Cell-Penetrating Peptide for Protein Delivery," *ACS Omega* 9 (2024): 19051–19056.

21. L. C. Dang, F. D. Melandri, and R. L. Stein, "Kinetic and Mechanistic Studies on the Hydrolysis of Ubiquitin C-Terminal 7-Amido-4-Methylcoumarin by Deubiquitinating Enzymes," *Biochemistry* 37 (1998): 1868–1879.

22. Y.-T. Li, J. Liang, J.-B. Li, G.-M. Fang, Y. Huang, and L. Liu, "New Semi-Synthesis of Ubiquitin C-Terminal Conjugate With 7-Amino-4-Methylcoumarin," *Journal of Peptide Science* 20 (2014): 102–107.

23. J. Fan, Y. Ye, G. Chu, et al., "Semisynthesis of Ubiquitin and SUMO-Rhodamine 110-Glycine Through Aminolysis of Boc-Protected Thioester Counterparts," *Journal of Organic Chemistry* 84 (2019): 14861–14867.

24. J. S. Suh, J. Y. Lee, G. Lee, C. P. Chung, and Y. J. Park, "Simultaneous Imaging and Restoration of Cell Function Using Cell Permeable Peptide Probe," *Biomaterials* 35 (2014): 6287–6298.

25. N. Safa, J. H. Pettigrew, T. J. Gauthier, and A. T. Melvin, "Direct Measurement of Deubiquitinating Enzyme Activity in Intact Cells Using a Protease-Resistant, Cell-Permeable, Peptide-Based Reporter," *Biochemical Engineering Journal* 151 (2019): 107320.

26. F. Loison, P. Nizard, T. Sourisseau, et al., "A Ubiquitin-Based Assay for the Cytosolic Uptake of Protein Transduction Domains," *Molecular Therapy* 11 (2005): 205–214.

27. D. S. Hameed, A. Sapmaz, L. Gjonaj, R. Merkx, and H. Ovaa, "Enhanced Delivery of Synthetic Labelled Ubiquitin Into Live Cells by Using Next-Generation Ub–TAT Conjugates," *Chembiochem* 19 (2018): 2553–2557.

28. W. Gui, S. Shen, and Z. Zhuang, "Photocaged Cell-Permeable Ubiquitin Probe for Temporal Profiling of Deubiquitinating Enzymes," *Journal of the American Chemical Society* 142 (2020): 19493–19501.

29. L.-J. Liang, Y. Wang, X. Hua, et al., "Cell-Permeable Stimuli-Responsive Ubiquitin Probe for Time-Resolved Monitoring of Substrate Ubiquitination in Live Cells," *JACS Au* 3 (2023): 2873–2882.

30. M. Jbara, S. Laps, S. K. Maity, and A. Brik, "Palladium-Assisted Cleavage of Peptides and Proteins Containing a Backbone With Thiazolidine Linkage," *Chemistry--A European Journal* 22 (2016): 14851–14855.

31. S. K. Singh, I. Sahu, S. M. Mali, et al., "Synthetic Uncleavable Ubiquitinated Proteins Dissect Proteasome Deubiquitination and Degradation, and Highlight Distinctive Fate of Tetraubiquitin," *Journal of the American Chemical Society* 138 (2016): 16004–16015.

32. G. Mann, G. Satish, P. Sulkshane, S. Mandal, M. H. Glickman, and A. Brik, "Synthesis and Delivery of a Stable Phosphorylated Ubiquitin Probe to Study Ubiquitin Conjugation in Mitophagy," *Chemical Communications* 57 (2021): 9438–9441.

33. S. Mandal and A. Brik, "Probing the Cell Delivery of Synthetic Diubiquitin Chains," *Chemical Communications* 58 (2022): 8782–8785.

34. G. Mann, P. Sadhu, and A. Brik, "Multiplexed Delivery of Synthetic (Un)conjugatable Ubiquitin and SUMO2 Enables Simultaneous Monitoring of Their Localization and Function in Live Cells," *Chembiochem* 23 (2022): e202200122.

35. A. Saha, S. Mandal, J. V. V. Arafiles, J. Gómez-González, C. P. R. Hackenberger, and A. Brik, "Structure–Uptake Relationship Study of DABCYL Derivatives Linked to Cyclic Cell-Penetrating Peptides for Live-Cell Delivery of Synthetic Proteins," *Angewandte Chemie, International Edition* 61 (2022): e202207551.

36. W. P. R. Verdurmen, M. Mazlami, and A. Plückthun, "A Quantitative Comparison of Cytosolic Delivery via Different Protein Uptake Systems," *Scientific Reports* 7 (2017): 13194.

37. P. G. Dougherty, A. Sahni, and D. Pei, "Understanding Cell Penetration of Cyclic Peptides," *Chemical Reviews* 119 (2019): 10241–10287.

38. L. Yan and M. E. Adams, "Lycotoxins, Antimicrobial Peptides From Venom of the Wolf Spider *Lycosa carolinensis*," *Journal of Biological Chemistry* 273 (1998): 2059–2066.

39. M. Akishiba, T. Takeuchi, Y. Kawaguchi, et al., "Cytosolic Antibody Delivery by Lipid-Sensitive Endosomolytic Peptide," *Nature Chemistry* 9 (2017): 751–761.

40. M. Akishiba and S. Futaki, "Inducible Membrane Permeabilization by Attenuated Lytic Peptides: A New Concept for Accessing Cell Interiors Through Ruffled Membranes," *Molecular Pharmaceutics* 16 (2019): 2540–2548.

41. Y. Nomura, K. Sakamoto, M. Akishiba, T. Iwata, H. Hirose, and S. Futaki, "Improved Cytosolic Delivery of Macromolecules Through Dimerization of Attenuated Lytic Peptides," *Bioorganic & Medicinal Chemistry Letters* 30 (2020): 127362.

42. B. Becker, S. Englert, H. Schneider, et al., "Multivalent Dextran Hybrids for Efficient Cytosolic Delivery of Biomolecular Cargoes," *Journal of Peptide Science* 27 (2021): e3298.

43. R. Feng, R. Ni, and Y. Chau, "Fusogenic Peptide Modification to Enhance Gene Delivery by Peptide-DNA Nano-Coassemblies," *Biomaterials Science* 10 (2022): 5116–5120.

44. K. Shinga, T. Iwata, K. Murata, et al., "L17ER$_4$: A Cell-Permeable Attenuated Cationic Amphiphilic Lytic Peptide," *Bioorganic & Medicinal Chemistry* 61 (2022): 116728.

45. S. Okano, Y. Kawaguchi, K. Kawano, H. Hirose, M. Imanishi, and S. Futaki, "Split Luciferase-Based Estimation of Cytosolic Cargo Concentration Delivered Intracellularly via Attenuated Cationic Amphiphilic Lytic Peptides," *Bioorganic & Medicinal Chemistry Letters* 72 (2022): 128875.

46. J. B. Giancola, J. B. Grimm, J. V. Jun, Y. D. Petri, L. D. Lavis, and R. T. Raines, "Evaluation of the Cytosolic Uptake of HaloTag Using a pH-Sensitive Dye," *ACS Chemical Biology* 19 (2024): 908–915.

47. A. Okon, J. Yang, J. B. Giancola, et al., "Facile Access to Branched Multispecific Proteins," *Bioconjugate Chemistry* 35 (2024): 954–962.

48. J. B. Giancola and R. T. Raines, "Endosomolytic Peptides Enable the Cellular Delivery of Peptide Nucleic Acids," *Chemical Communications* 60 (2024): 15019–15022.

49. J. Du, S. Babik, Y. Li, et al., "A Cryptic K48 Ubiquitin Chain Binding Site on UCH37 Is Required for Its Role in Proteasomal Degradation," *eLife* 11 (2022): e76100.

50. A. B. Schroeder, E. T. A. Dobson, C. T. Rueden, P. Tomancak, F. Jug, and K. W. Eliceiri, "The ImageJ Ecosytstem: Open-Source Software for Image Visualization, Processing, and Analysis," *Protein Science* 30 (2021): 234–249.

51. T. A. M. Groothuis, N. P. Dantuma, J. Neefjes, and F. A. Salomons, "Ubiquitin Crosstalk Connecting Cellular Processes," *Cell Division* 1 (2006): 21.

52. N. P. Dantuma, T. A. M. Groothuis, F. A. Salomons, and J. Neefjes, "A Dynamic Ubiquitin Equilibrium Couples Proteasomal Activity to Chromatin Remodeling," *Journal of Cell Biology* 173 (2006): 19–26.

53. D. H. Lee and A. L. Goldberg, "Proteasome Inhibitors: Valuable New Tools for Cell Biologists," *Trends in Cell Biology* 8 (1998): 397–403.

Supporting Information

Additional supporting information can be found online in the Supporting Information section.